The Astrophysical Journal, 740:121 (8pp), 2011 October 20 doi:10.1088/0004-637X/740/2/121

ASTROMETRIC IMAGE CENTROID DISPLACEMENTS DUE TO GRAVITATIONAL MICROLENSING BY THE ELLIS WORMHOLE

Yukiharu Toki[1], Takao Kitamura[1], Hideki Asada[1], and Fumio Abe[2,3]
[1] Faculty of Science and Technology, Hirosaki University, Hirosaki 036-8561, Japan
[2] Solar-Terrestrial Environment Laboratory, Nagoya University Furo-cho, Chikusa-ku, Nagoya 464-8601, Japan; abe@stelab.nagoya-u.ac.jp
Received 2011 April 26; accepted 2011 July 22; published 2011 October 4

ABSTRACT

Continuing work initiated in an earlier publication, we study the gravitational microlensing effects of the Ellis wormhole in the weak-field limit. First, we find a suitable coordinate transformation, such that the lens equation and analytic expressions of the lensed image positions can become much simpler. Second, we prove that two images always appear for the weak-field lens by the Ellis wormhole. By using these analytic results, we discuss astrometric image centroid displacements due to gravitational microlensing by the Ellis wormhole. The astrometric image centroid trajectory by the Ellis wormhole is different from the standard one by a spherical lensing object that is expressed by the Schwarzschild metric. The anomalous shift of the image centroid by the Ellis wormhole lens is smaller than that by the Schwarzschild lens, provided that the impact parameter and the Einstein ring radius are the same. Therefore, the lensed image centroid by the Ellis wormhole moves slower. Such a difference, although it is very small, will be, in principle, applicable for detecting or constraining the Ellis wormhole by using future high-precision astrometry observations. In particular, the image centroid position gives us additional information, so that the parameter degeneracy existing in photometric microlensing can be partially broken. The anomalous shift reaches the order of a few micro arcseconds, if our galaxy hosts a wormhole with throat radius larger than 10^5 km. When the source moves tangentially to the Einstein ring, for instance, the maximum position shift of the image centroid by the Ellis wormhole is 0.18 normalized by the Einstein ring radius. For the same source trajectory, the maximum difference between the centroid displacement by the Ellis wormhole lens and that by the Schwarzschild one with the same Einstein ring radius is -0.16 in the units of the Einstein radius, where the negative means that the astrometric displacement by the Ellis wormhole lens is smaller than that by the Schwarzschild one.

Key words: gravitational lensing: micro

Online-only material: color figures

1. INTRODUCTION

A peculiar feature of general relativity is that the theory admits a nontrivial topology of a spacetime. A solution of the Einstein equation that connects distant points of space–time was introduced by Einstein & Rosen (1935). This solution called the *Einstein–Rosen bridge* was the first solution to later be referred to as a wormhole. Initially, this type of solution was just a trivial or teaching example of mathematical physics. However, Morris & Thorne (1988) proved that some wormholes are "traversable," i.e., space and time travel can be achieved by passing through the wormholes. They also showed that the existence of a wormhole requires exotic matter that violates the null energy condition. The existence of wormholes, though they are very exotic, has not been ruled out in theory. Inspired by the Morris–Thorne paper, a number of theoretical works (see Visser (1995); Lobo (2007), and references therein) on wormholes have been done. The curious nature of wormholes such as time travel, negative energy conditions, space–time foams, and growth of a wormhole in an accelerating universe have been studied. In spite of enthusiastic theoretical investigations, studies searching for observational evidence of the existence of wormholes are scarce. Only a few attempts have been made to show the existence or the nonexistence of wormholes in our universe (Cramer et al. 1995; Torres et al. 1998; Safonova et al. 2002; Bogdanov & Cherepashchuk 2008).

A possible observational method that has been proposed to detect or exclude the existence of wormholes is the application of optical gravitational lensing, since the light ray propagation is sensitive to a local spacetime geometry. The gravitational lensing of wormholes was pioneered by Cramer et al. (1995), who inferred that some wormholes show "negative-mass" lensing. They showed that the light curve of the negative-mass lensing event of a distant star has singular double peaks. Several authors subsequently conducted theoretical studies on detectability (Safonova et al. 2002; Bogdanov & Cherepashchuk 2008). Another gravitational lensing method employing gamma rays was proposed by Torres et al. (1998), who postulated that the singular negative-mass lensing of distant active galactic nuclei causes a sharp spike of gamma rays and may be observed as double-peaked gamma-ray bursts. They analyzed BATSE data to put an upper limit to the negative-mass density $O(10^{-36})$ g cm^{-3} in the form of wormhole-like objects.

There have been several recent works (Shatskiĭ 2004; Perlick 2004; Nandi et al. 2006; Rahaman 2007; Dey & Sen 2008; Abe 2010; Asada 2011) on the gravitational lensing of wormholes as structures of space–time. Such studies are expected to unveil lensing properties directly from the space–time structure. One study Dey & Sen (2008) calculated the deflection angle of light due to the Ellis wormhole, whose asymptotic mass at infinity is zero. The massless wormhole is particularly interesting because it is expected to have unique gravitational lensing effects. This type of wormhole was first introduced by Ellis (1973) as a massless scalar field. Later, Morris & Thorne (1988) studied this

[3] Nagoya University Southern Observatories

wormhole and proved it to be traversable. The dynamical feature was studied by Shinkai & Hayward (2002), who showed that Gaussian perturbation causes either explosion to an inflationary universe or collapse to a black hole. Das & Kar (2005) showed that the tachyon condensate can be a source for the Ellis geometry. Abe (2010) provided a method to calculate light curves of the gravitational microlensing of the Ellis wormhole in the weak-field limit. This result has been discussed as one example of corrections to the standard formula of the deflection angle by Asada (2011).

The main results of this paper are: (1) We derive analytic expressions for calculations of the wormhole lensing. (2) We show the astrometric image centroid trajectory by the Ellis wormhole lens. Studies of centroid displacements of lensed images have been limited within the Schwarzschild lens (Walker 1995; Miyamoto & Yoshii 1995; Hosokawa et al. 1997; Safizadeh et al. 1999; Jeong et al. 1999; Asada 2002; Han & Lee 2002). In Section 2, we discuss gravitational lensing by the Ellis wormhole in the weak-field limit. We use a suitable coordinate transformation, such that the lens equation to determine image positions can take a much simpler form than the previous one derived by Abe (2010). By using this method, calculations of the gravitational microlensing by the Ellis wormhole are shortened. In addition, we prove that two images always appear for the weak-field lens by the Ellis wormhole. In Section 3, we discuss astrometric image centroid displacements due to gravitational microlensing by the Ellis wormhole. The results are summarized in Section 4.

2. GRAVITATIONAL LENSING BY THE ELLIS WORMHOLE: WEAK-FIELD APPROXIMATION

2.1. Ellis Wormhole Lens

Magnification of the apparent brightness of a distant star by the gravitational lensing effect of another star was predicted by Einstein (1936). This kind of lensing effect is called "microlensing" because the images produced by the gravitational lensing are very close to each other and are difficult for the observer to resolve. The observable effects are not only the changing apparent brightness of the source star but also the shift in the image centroid position. The brightness changing effect was discovered in 1993 (Udalski et al. 1993; Alcock et al. 1993; Aubourg et al. 1993) and has been used to detect astronomical objects that do not emit observable signals (such as visible light, radio waves, and X-rays) or are too faint to observe. Microlensing has successfully been applied to detect extrasolar planets (Bond et al. 2004; Beaulieu et al. 2006) and brown dwarfs (Calchi Novati et al. 2009; Gould et al. 2009). Microlensing is also used to search for unseen black holes (Alcock et al. 2001; Bennett et al. 2002; Poindexter et al. 2005) and massive compact halo objects (Alcock et al. 2000; Tisserand et al. 2007; Wyrzykowski et al. 2009), a candidate for dark matter.

The gravity of a star is well expressed by the Schwarzschild metric. The gravitational microlensing of the Schwarzschild metric (Refsdal 1964; Liebes 1964; Paczyński 1986) has been studied in the weak-field limit. In this section, we simply follow the method used for Schwarzschild lensing. Figure 1 shows the relation between the source star, the lens (wormhole), and the observer. The Ellis wormhole is known to be a massless wormhole, which means that the asymptotic mass at infinity is zero. The Ellis wormhole is expressed by the line element

$$ds^2 = dt^2 - dr^2 - (r^2 + a^2)(d\theta^2 + \sin^2(\theta)d\phi^2), \qquad (1)$$

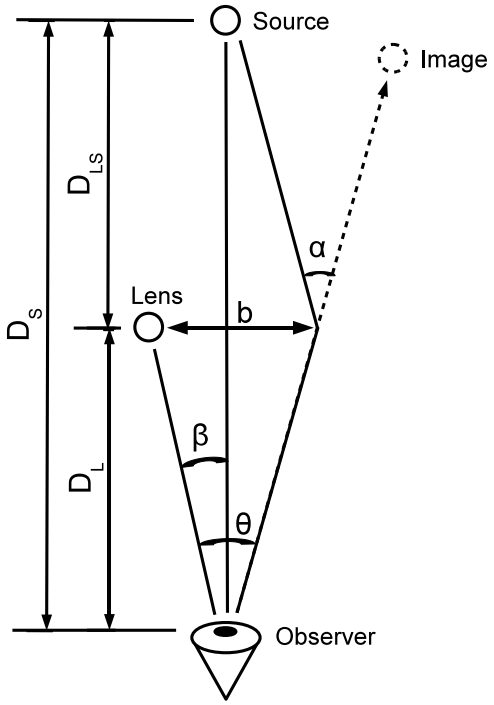

Figure 1. Sketch of the relation between the source star, the lens (wormhole), and the observer.

where a is the throat radius of the wormhole. However, this wormhole deflects light by gravitational lensing (Clément 1984; Chetouani & Clément 1984; Nandi et al. 2006; Dey & Sen 2008) because of its curved space–time structure.

The deflection angle $\alpha(r)$ of the Ellis wormhole was derived by Dey & Sen (2008) to be

$$\alpha(r) = \pi \left\{ \sqrt{\frac{2(r^2 + a^2)}{2r^2 + a^2}} - 1 \right\}, \qquad (2)$$

where r is the closest approach of the light. In the weak-field limit ($r \to \infty$), the deflection angle becomes

$$\alpha(r) \to \frac{\pi}{4}\frac{a^2}{r^2} + o\left(\frac{a}{r}\right)^4. \qquad (3)$$

Note that the Dey & Sen (2008) treatment is true for the weak-field region but it may be corrected in the strong-field one, because they assumed that $r = 0$ was singular and it could be excluded as is the case for the Schwarzschild metric. For the Ellis wormhole, however, $r = 0$ is not a singularity but a regular sphere and hence $r = 0$ cannot be excluded in the strong-field lensing.

The angle between the lens (wormhole) and the source β can then be written as

$$\beta = \frac{1}{D_L}b - \frac{D_{\rm LS}}{D_S}\alpha(r), \qquad (4)$$

where D_L, D_S, $D_{\rm LS}$, and b are the distances from the observer to the lens, from the observer to the source, and from the lens to the source, and the impact parameter of the light, respectively. In the asymptotic limit, Schwarzschild lensing and massive Janis–Newman–Winnicour (JNW) wormhole lensing (Dey & Sen 2008) have the same leading term of $o(1/r)$. Therefore, the lensing property of the JNW wormhole is approximately

the same as that of Schwarzschild lensing and is difficult to distinguish. As shown in Equation (3), the deflection angle of the Ellis wormhole does not have the term of $o(1/r)$ and starts from $o\left(1/r^2\right)$. This is due to the massless nature of the Ellis wormhole and indicates the possibility of observational discrimination from the ordinary gravitational lensing effect. In the weak-field limit, b is approximately equal to the closest approach r. For the Ellis wormhole, $b = \sqrt{r^2 + a^2} \to r(r \to \infty)$. We thus obtain

$$\beta = \frac{r}{D_L} - \frac{\pi}{4}\frac{D_{\rm LS}}{D_S}\frac{a^2}{r^2} \qquad (r > 0). \tag{5}$$

The light passing through the other side of the lens may also form images. However, Equation (5) represents deflection in the wrong direction at $r < 0$. Thus, we must change the sign of the deflection angle:

$$\beta = \frac{r}{D_L} + \frac{\pi}{4}\frac{D_{\rm LS}}{D_S}\frac{a^2}{r^2} \qquad (r < 0). \tag{6}$$

It would be useful to note that a single equation is suitable both for $r > 0$ and $r < 0$ images in the Schwarzschild lensing. However, such treatment is applicable only when the deflection angle is an odd function of r.

If the source and lens are completely aligned along the line of sight, the image is expected to be circular (an Einstein ring). The Einstein radius R_E, which is defined as the radius of the circular image on the lens plane, is obtained from Equation (5) with $\beta = 0$ as

$$R_E = \sqrt[3]{\frac{\pi}{4}\frac{D_L D_{\rm LS}}{D_S}a^2}. \tag{7}$$

The image positions can then be calculated from

$$\beta = \theta - \frac{\theta_E^3}{\theta^2} \qquad (\theta > 0) \tag{8}$$

and

$$\beta = \theta + \frac{\theta_E^3}{\theta^2} \qquad (\theta < 0), \tag{9}$$

where $\theta = b/D_L \approx r/D_L$ is the angle between the image and lens, and $\theta_E = R_E/D_L$ is the angular Einstein radius. Using reduced parameters $\hat{\beta} = \beta/\theta_E$ and $\hat{\theta} = \theta/\theta_E$, Equations (8) and (9) become simple cubic formulae:

$$\hat{\theta}^3 - \hat{\beta}\hat{\theta}^2 - 1 = 0 \qquad (\hat{\theta} > 0) \tag{10}$$

and

$$\hat{\theta}^3 - \hat{\beta}\hat{\theta}^2 + 1 = 0 \qquad (\hat{\theta} < 0). \tag{11}$$

Following Abe (2010), first, we briefly summarize how to obtain the roots of the above equations. As the discriminant of Equation (10) is $-4\hat{\beta}^3 - 27 < 0$, Equation (10) has two conjugate complex solutions and a real solution:

$$\hat{\theta} = \frac{\hat{\beta}}{3} + U_{1+} + U_{1-}, \tag{12}$$

with

$$U_{1\pm} = \sqrt[3]{\frac{\hat{\beta}^3}{27} + \frac{1}{2} \pm \sqrt{\frac{1}{4}\left(1 + \frac{2\hat{\beta}^3}{27}\right)^2 - \frac{\hat{\beta}^6}{27^2}}}. \tag{13}$$

The real positive solution corresponds to the physical image.

The discriminant of Equation (11) is $4\hat{\beta}^3 - 27$. Thus it has a real solution if $\hat{\beta} < \sqrt[3]{27/4}$:

$$\hat{\theta} = \frac{\hat{\beta}}{3} + U_{2+} + U_{2-}, \tag{14}$$

where

$$U_{2\pm} = \omega\sqrt[3]{\frac{\hat{\beta}^3}{27} - \frac{1}{2} \pm \sqrt{\frac{1}{4}\left(1 - \frac{2\hat{\beta}^3}{27}\right)^2 - \frac{\hat{\beta}^6}{27^2}}}, \tag{15}$$

with $\omega \equiv e^{(2\pi/3)i}$. This solution corresponds to a physical image inside the Einstein ring. For $\hat{\beta} > \sqrt[3]{27/4}$, Equation (11) has three real solutions. However, two of them are not physical because they do not satisfy $\hat{\theta} < 0$. Only the solution

$$\hat{\theta} = \frac{\hat{\beta}}{3} + \omega U_{2+} + U_{2-} \tag{16}$$

corresponds to a physical image inside the Einstein ring.

In both cases of $\hat{\theta} > 0$ and $\hat{\theta} < 0$, careful treatments of $\hat{\beta}$ inside the square roots and the cube roots are required in order to know whether they are a real positive, real negative, or complex.

2.2. Simplified Expressions of Lensed Image Positions

Next, let us consider an appropriate coordinate transformation as

$$u \equiv \frac{1}{\hat{\theta}}, \tag{17}$$

so that Equations (10) and (11) can be rewritten respectively as

$$u^3 + \hat{\beta}u - 1 = 0 \qquad (u > 0) \tag{18}$$

and

$$u^3 - \hat{\beta}u + 1 = 0 \qquad (u < 0). \tag{19}$$

Note that these equations take exactly the standard form called *depressed cubic* for using Cardano's method to find analytic roots of a cubic equation. In next subsetion, it is proven that there exists the only one true root for each equation. Hence, we immediately get the unique real root for $u > 0$ as

$$u_1 = \frac{1}{\hat{\theta}_1} = \sqrt[3]{\frac{1}{2} + \sqrt{\frac{1}{4} + \frac{\hat{\beta}^3}{27}}} - \sqrt[3]{-\frac{1}{2} + \sqrt{\frac{1}{4} + \frac{\hat{\beta}^3}{27}}}, \tag{20}$$

and the unique real one for $u < 0$ as

$$u_2 = \frac{1}{\hat{\theta}_2} = -\sqrt[3]{\frac{1}{2} + \sqrt{\frac{1}{4} - \frac{\hat{\beta}^3}{27}}} - \sqrt[3]{\frac{1}{2} - \sqrt{\frac{1}{4} - \frac{\hat{\beta}^3}{27}}}. \tag{21}$$

Clearly it can be shown by direct but lengthy calculations that Equations (20) and (21) agree with Equations (12) and (14), respectively. Note that they are much simpler than Equations (12)

and (14). In particular, these improved expressions make it much easier to see the sign of the argument of the square root and the cube one compared with Equations (12) and (14). For $\hat{\beta} > \sqrt[3]{27/4}$, the argument of the square root in Equation (21) is always negative, so that Equation (21) can be rewritten as

$$u_2 = -2\sqrt{\frac{\hat{\beta}}{3}}\cos\left[\frac{1}{3}\arctan\left(2\sqrt{\frac{\hat{\beta}^3}{27}-\frac{1}{4}}\right)\right]. \quad (22)$$

Here we used a relation for two real numbers $p > 0$ and $q < 0$ as

$$\sqrt[3]{p+\sqrt{q}}+\sqrt[3]{p-\sqrt{q}} = 2\sqrt[3]{r}\cos\left[\frac{1}{3}\arctan\left(\frac{\sqrt{-q}}{p}\right)\right]. \quad (23)$$

This relation can be shown as follows. For $p > 0$ and $q < 0$, we can put $p+\sqrt{q} = r\exp(i\phi)$ by introducing a radial distance defined as $r \equiv \sqrt{p^2-q}$ and an angle coordinate defined as $\tan\phi \equiv p^{-1}\sqrt{-q}$. From its complex conjugate we obtain $p-\sqrt{q} = r\exp(-i\phi)$. Hence we get

$$\sqrt[3]{p+\sqrt{q}} = \sqrt[3]{r}\exp(i\phi/3), \quad (24)$$

$$\sqrt[3]{p-\sqrt{q}} = \sqrt[3]{r}\exp(-i\phi/3), \quad (25)$$

both of which are combined to get Equation (23).

2.3. Number of Images Lensed by the Ellis Wormhole

It is not convenient to use Cardano's formulae to know how many images appear for the Ellis wormhole lens, because the formulae include a combination of square roots and cube ones and therefore straightforward but lengthy calculations are required to know the sign of the argument of the roots.

In order to bypass such difficulties, we use Descartes' rule of signs (e.g., Waerden (1966)), which states that the number of positive roots either equals that of sign changes in coefficients of a polynomial (ignoring powers which do not appear) or less than it by a multiple of two. This theorem tells that Equations (10) and (18) have the only one positive root, because the sign of the coefficient of each power (ignoring powers which do not appear) is +, −, − for Equation (10) and +, +, − for Equation (18). For Equations (11) and (19), we make a parity transformation as $\hat{\theta}' = -\hat{\theta}$ and $\hat{u}' = -\hat{u}$, so that we can directly apply the Descartes' theorem. After the parity transformation is made for Equations (11) and (19), the sign of the coefficient of each power is −, −, + for Equation (11) and −, +, + for Equation (19). Therefore, we have the only one negative root for each of Equations (11) and (19).

The left-hand side of Equation (18) becomes -1 and $\beta \geqslant 0$ for $u = 0$ and 1, respectively. The continuity of the left-hand side thus means that the positive root u_1 and $\hat{\theta}_1$ satisfy

$$0 < u_1 \leqslant 1, \quad (26)$$

$$1 \leqslant \hat{\theta}_1 < +\infty, \quad (27)$$

respectively. The left-hand side of Equation (19) becomes $-\infty$ and $\beta \geqslant 0$ for $u = -\infty$ and -1, respectively. Hence, the continuity of the left-hand side means that the negative root u_2 and $\hat{\theta}_2$ satisfy

$$u_2 \leqslant -1, \quad (28)$$

$$-1 \leqslant \hat{\theta}_2 < 0, \quad (29)$$

respectively. The above inequalities on $\hat{\theta}_1$ and $\hat{\theta}_2$ hold also for the Ellis wormhole similarly to the Schwarzschild lens.

3. ASTROMETRIC IMAGE CENTROID DISPLACEMENTS BY THE ELLIS WORMHOLE

The light curve of Schwarzschild lensing was derived by Paczyński (1986), whereas the counterpart by the Ellis wormhole was calculated by Abe (2010). The magnification of the brightness for each image by the Ellis wormhole lens is

$$A_1 \equiv \left|\frac{\hat{\theta}_1}{\hat{\beta}}\frac{d\hat{\theta}_1}{d\hat{\beta}}\right| = \frac{1}{\left(1-\frac{1}{\hat{\theta}_1^3}\right)\left(1+\frac{2}{\hat{\theta}_1^3}\right)} = \frac{1}{\left(1-u_1^3\right)\left(1+2u_1^3\right)}, \quad (30)$$

$$A_2 \equiv \left|\frac{\hat{\theta}_2}{\hat{\beta}}\frac{d\hat{\theta}_2}{d\hat{\beta}}\right| = \frac{1}{\left(1+\frac{1}{\hat{\theta}_2^3}\right)\left(\frac{2}{\hat{\theta}_2^3}-1\right)} = \frac{1}{\left(1+u_2^3\right)\left(2u_2^3-1\right)}, \quad (31)$$

where A_1 and A_2 are magnification of the outer and inner images, $\hat{\theta}_1$ and $\hat{\theta}_2$ correspond to outer and inner images, respectively. Here, we use $0 < u_1 \leqslant 1$ and $u_2 \leqslant -1$. Hence, the total magnification of the brightness A is

$$A \equiv A_1 + A_2 = \frac{1}{\left(1-u_1^3\right)\left(1+2u_1^3\right)} + \frac{1}{\left(1+u_2^3\right)\left(2u_2^3-1\right)}. \quad (32)$$

The relation between the lens and source trajectory in the sky is shown in Figures 2 and 3. The time dependence of $\hat{\beta}$ is

$$\hat{\beta}(t) = \sqrt{\hat{\beta}_0^2 + (t-t_0)^2/{t_E}^2}, \quad (33)$$

where $\hat{\beta}_0$ is the impact parameter of the source trajectory and t_0 is the time of closest approach. t_E is the Einstein radius crossing time given by

$$t_E = R_E/v_T, \quad (34)$$

where v_T is the transverse velocity of the lens relative to the source and observer. The light curves obtained from Equations (32) and (33) are shown as thick red lines in Figure 4. The light curves corresponding to Schwarzschild lensing are shown as thin blue lines for comparison. Abe (2010) found that the magnifications by the Ellis wormhole are generally less than those of Schwarzschild lensing. The light curve of the Ellis wormhole for $\hat{\beta}_o < 1.0$ shows characteristic gutters on both sides of the peak immediately outside the Einstein

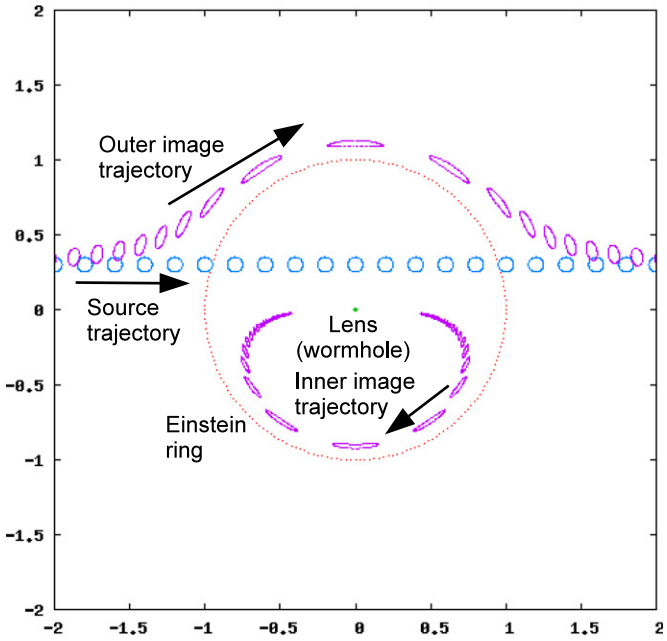

Figure 2. Source and image trajectories in the sky from the position of the observer.

(A color version of this figure is available in the online journal.)

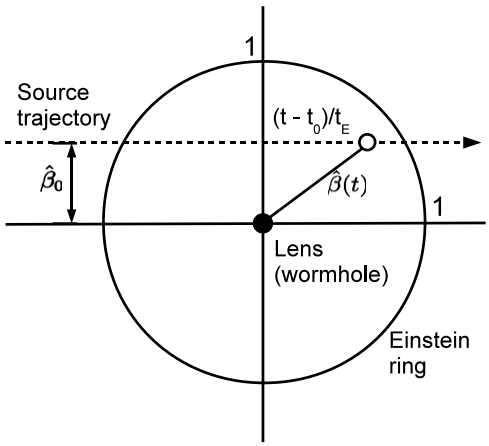

Figure 3. Sketch of the relation between the source trajectory and the lens (wormhole) in the sky. All quantities are normalized by the angular Einstein radius θ_E.

ring crossing times ($t = t_0 \pm t_E$). The depth of the gutters is about 4% from the baseline. Amazingly, the star becomes fainter than normal in terms of apparent brightness in the gutters. This means that the Ellis wormhole lensing has off-center divergence. In conventional gravitational lensing theory (Schneider et al. 1992), the convergence of light is expressed by a convolution of the surface mass density. Thus, we need to introduce negative mass to describe a diverging lens (like a concave lens in optics) by the Ellis wormhole. However, negative mass is not a physical entity. Since the lensing by the Ellis wormhole is converging at the center, lensing at some other place must be diverging because the wormhole has zero asymptotic mass and hence converging and diverging effects are compensated for each other in total.

For $\hat{\beta}_o > 1.0$, the light curve of the wormhole has a basin at t_0 and no peak. Using these features, discrimination from Schwarzschild lensing can be achieved. Equations (7) and (34) indicate that physical parameters (D_L, a, and v_T) are degenerate in t_E and cannot be derived by fitting the light curve data. This situation is the same as that for Schwarzschild lensing. To obtain or constrain these values, observations of the finite-source effect (Nemiroff & Wickramasinghe 1994) or parallax (Alcock et al. 1995) are necessary. Astrometry gives a method for breaking the degeneracy as discussed later.

In analogy with the center of the mass distribution, the centroid position of the light distribution of a gravitationally microlensed source is given by

$$\hat{\theta}_{pc} = \frac{A_1\hat{\theta}_1 + A_2\hat{\theta}_2}{A}. \tag{35}$$

In making numerical figures, we employ x–y coordinates in the way that the center is chosen as the location of the Ellis wormhole, the x-axis is taken along the direction of the source motion and the y-axis is perpendicular to the source motion. See Figure 5 for the image centroid trajectories for $\hat{\beta}_0 = 0.2, 0.5, 1.0, 1.5$. For each $\hat{\beta}_0$, the respective maximum differences between the image centroid position by the Ellis wormhole and that by the Schwarzschild one are -0.03, -0.08, -0.16, -0.20 in the units of the Einstein ring radius, respectively. This implies that the astrometric lensing by the Ellis wormhole is relatively weaker than that by the Schwarzschild one.

In the weak-field region, the suppression of the anomalous shift of the image centroid position is because the bending angle by the Ellis wormhole is proportional to the inverse squared impact parameter, whereas that by the Schwarzschild lens depends on the inverse impact parameter. Figure 6 shows the relative displacement of the image centroid with respect to the source position that is assumed to be in uniform linear motion. The maximum vertical displacements are 0.06, 0.14, 0.18, 0.15 for $\hat{\beta}_0 = 0.2, 0.5, 1.0, 1.5$, respectively. Here, a key question is whether the Ellis lensing and the Schwarzschild one are distinguished from the centroid displacement curve. The relative displacement trajectory by the Schwarzschild lens is known to be an ellipse (Walker 1995; Jeong et al. 1999). It is natural to ask whether the displacement curve by the Ellis wormhole lens is also an ellipse. Figure 6 shows that the relative trajectory by the Ellis lens looks like an ellipse but has a small difference. The shape is symmetric along the x-axis but slightly asymmetric along the y-axis like a tree leaf, particularly for $\hat{\beta}_0 = 0.2$. Figure 6, however, shows that such a deviation of the relative trajectory from elliptic orbits is very small. Another difference is that the relative displacement at large t, for instance $t = -20$ or 20, is dependent strongly on the Ellis lens or the Schwarzschild one. This is because the asymptotic behavior of the centroid displacement is different ($\hat{\beta}^{-2}$ or $\hat{\beta}^{-1}$). In other words, the displacement effect by the Ellis lens goes away faster. This suggests that a long-term observation including a tail part of the centroid curve is required to distinguish the Ellis lenses by astrometric observations alone.

The detectability of the image centroid displacements of the background star depends on the timescale called *the Einstein radius crossing time* t_E that depends on the transverse velocity v_T. There is no reliable estimate of v_T for wormholes. Following Abe (2010), we assume that the velocity of the wormhole is approximately equal to the rotation velocity of stars ($v_T = 220\,\mathrm{km\,s^{-1}}$) if it is bound to the Galaxy. If the wormhole is not bound to our Galaxy, the transverse velocity would be much higher. We assume $v_T = 5000\,\mathrm{km\,s^{-1}}$ (Safonova et al. 2002)

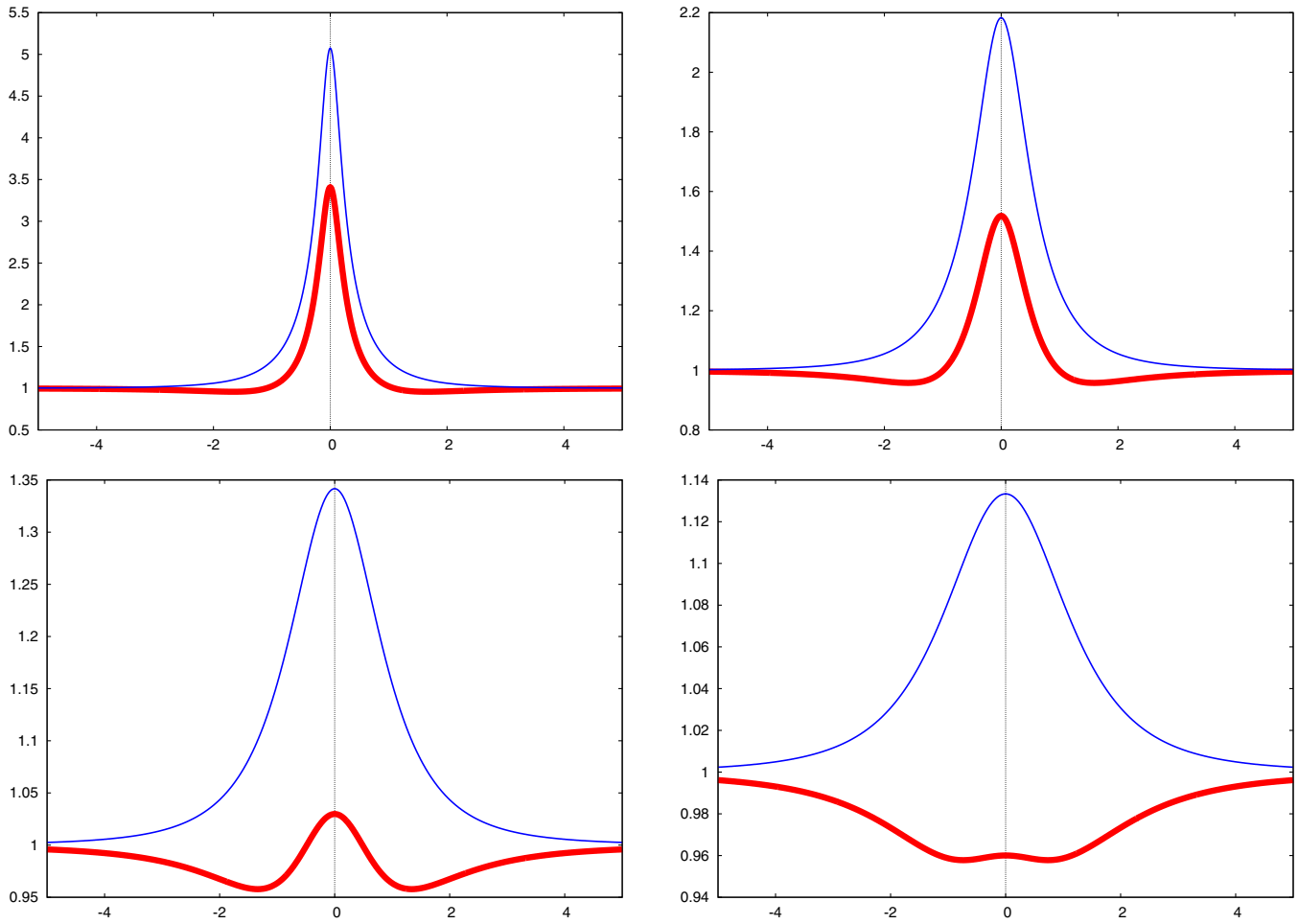

Figure 4. Light curves for $\hat{\beta}_0 = 0.2$ (top left), $\hat{\beta}_0 = 0.5$ (top right), $\hat{\beta}_0 = 1.0$ (bottom left), and $\hat{\beta}_0 = 1.5$ (bottom right). Thick red lines are for wormholes. Thin blue lines are corresponding light curves for Schwarzschild lenses. For light curves, the horizontal axis denotes time in units of the Einstein radius crossing time and the vertical one denotes the total magnification.

(A color version of this figure is available in the online journal.)

for the unbound wormhole. Table 1 shows the Einstein radius crossing times of the Ellis wormhole lensings for the Galactic bulge and LMC in both bound and unbound scenarios. As the frequencies of current microlensing observations are limited to once every few hours, an event for which the timescale is less than 1 day is difficult to detect. To find very long timescale events ($t_E \geqslant 1000$ days), long-term monitoring of events is necessary. The realistic period of observation is $\leqslant$10 years. Thus, the realistic size of the throat that we can search for is limited to 100 km $\leqslant a \leqslant 10^7$ km both for the Galactic bulge and LMC if wormholes are bound to our Galaxy. If wormholes are unbound, the detection is limited to 10^5 km $\leqslant a \leqslant 10^9$ km.

The detectability depends also on the angular shift due to the Ellis wormhole lens. The typical angular scale is $O(\theta_E)$. See Table 2 for the size of θ_E corresponding to various values of the throat radius. Near-future astrometry space missions such as *Gaia* and JASMINE are expected to have angular sensitivity of a few micro arcseconds, for which the detection is limited as $a \geqslant 10^2$ km. This limit is much weaker than that by the mission life time as 10^5 km $\leqslant a \leqslant 10^9$ km for unbound wormholes.

Note that there is a small difference in the image centroid position (and its motion with time) between the Scwarzschild lensing and the Ellis wormhole one. In practice, therefore, it is unlikely to detect the wormhole by astrometric observation

Table 1
Einstein Radius Crossing Times for Bulge and LMC Lensings

a (km)	Bulge[a] t_E (day)		LMC[b] t_E (day)	
	Bound[c]	Unbound[d]	Bound[c]	Unbound[d]
1	0.019	0.001	0.035	0.002
10	0.089	0.004	0.164	0.007
10^2	0.413	0.018	0.761	0.033
10^3	1.92	0.084	3.53	0.155
10^4	8.90	0.392	16.4	0.721
10^5	41.3	1.82	76.1	3.35
10^6	192	8.44	353	15.5
10^7	890	39.2	1639	72.1
10^8	4130	182	7608	335
10^9	$>10^4$	843	$>10^4$	1553
10^{10}	$>10^4$	3915	$>10^4$	7212

Notes. a is the throat radius of the wormhole, t_E is the Einstein radius crossing time.

[a] $D_S = 8$ kpc and $D_L = 4$ kpc are assumed.

[b] $D_S = 50$ kpc and $D_L = 25$ kpc are assumed.

[c] $v_T = 220\,\mathrm{km\,s^{-1}}$ is assumed.

[d] $v_T = 5000\,\mathrm{km\,s^{-1}}$ is assumed.

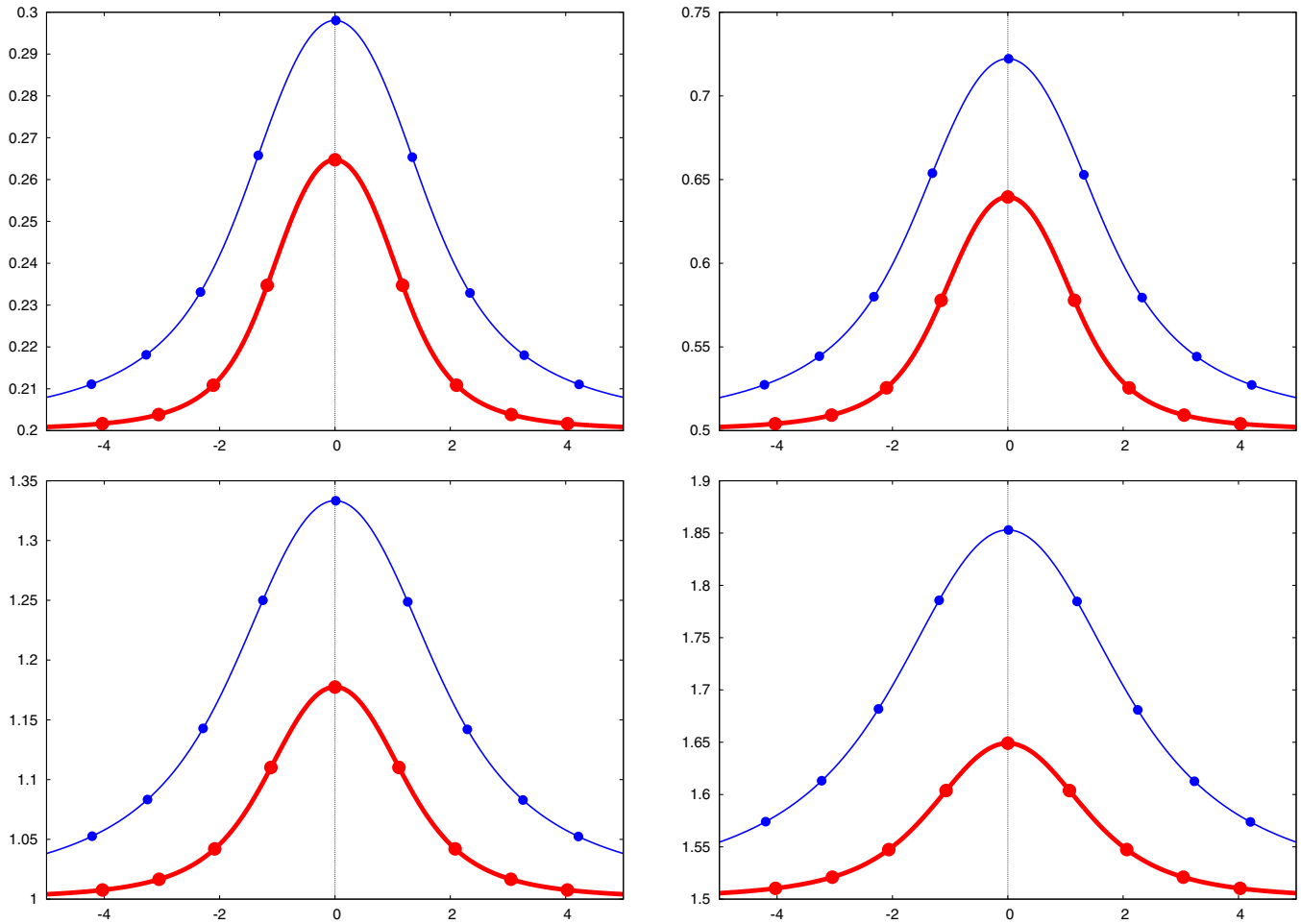

Figure 5. Image centroid trajectories both by the Ellis wormhole lens and by the Schwarzschild one with the same Einstein ring radius for $\hat{\beta}_0 = 0.2$ (top left), $\hat{\beta}_0 = 0.5$ (top right), $\hat{\beta}_0 = 1.0$ (bottom left), and $\hat{\beta}_0 = 1.5$ (bottom right). Thick red lines are image centroid orbits expressed as $(\hat{\theta}_{\mathrm{pc},x}(t), \hat{\theta}_{\mathrm{pc},y}(t))$ for wormholes. Thin blue lines correspond to Schwarzschild lens cases. The horizontal axis ($\hat{\theta}_{\mathrm{pc},x}$) is taken along the source motion and the vertical one ($\hat{\theta}_{\mathrm{pc},y}$) is normal to the direction of its motion. Scales are normalized by the Einstein ring radius, where we use Equation (35). In order to make the image centroid motion clear, we plot the image centroid position at $t = -4, -3, -2, -1, 0, 1, 2, 3, 4$, which are marked as filled disks in the figure. For the Ellis wormhole case, the lensed centroid moves slower than that for the Schwarzschild one, provided that the Einstein ring radius and the impact parameter are the same.

(A color version of this figure is available in the online journal.)

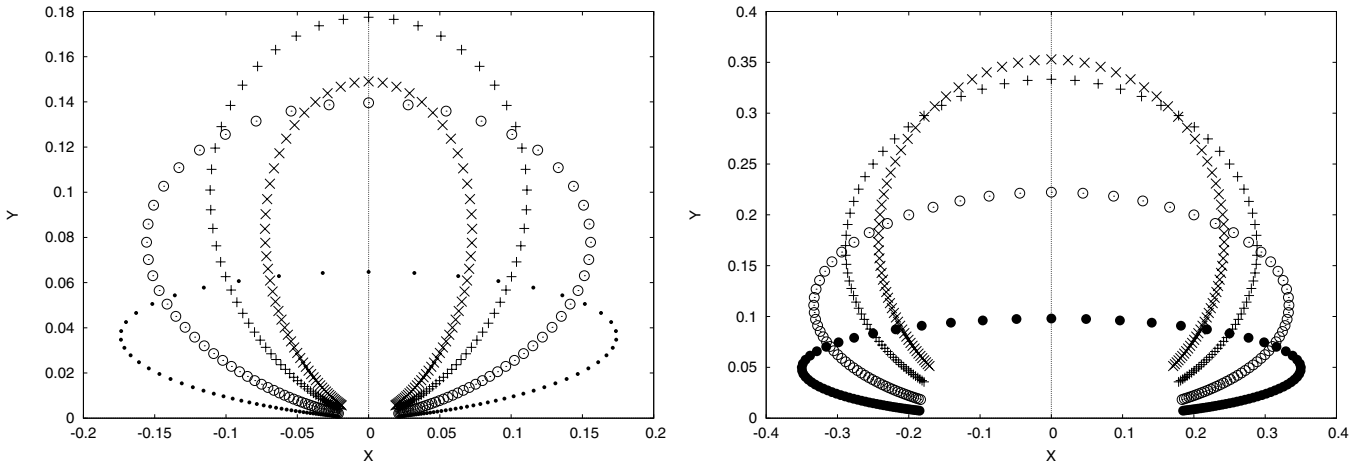

Figure 6. Relative displacements of the image centroid by the Ellis wormhole lens (left panel) and by the Schwarzschild one (right panel) with respect to the source position in uniform linear motion. The parameter values (normalized by the Einstein ring radius) are the same as those in Figure 5. The dot (·), circle (◯), plus (+), cross (×) denote the positions for $\hat{\beta}_0 = 0.2, 0.5, 1.0, 1.5$, respectively, where the horizontal axis denotes the direction of the source motion. Points are spaced uniformly in time as $\Delta t = 0.1$. In the limit of $t = \pm\infty$, these points approach the origin of the X–Y plane, namely, the image centroid position agrees with the source. Hence, points around the origin are very crowded and thus we omit the crowded points by choosing the time domain from $t = -20$ to 20.

Table 2
Einstein Radii for Bulge and LMC Lensings

a(km)	Bulge[a]		LMC[b]	
	R_E(km)	θ_E(mas)	R_E(km)	θ_E(mas)
1	3.64×10^5	0.001	6.71×10^5	<0.001
10	1.69×10^6	0.003	3.12×10^6	0.001
10^2	7.85×10^6	0.013	1.45×10^7	0.004
10^3	3.64×10^7	0.061	6.71×10^7	0.018
10^4	1.69×10^8	0.283	3.12×10^8	0.083
10^5	7.85×10^8	1.31	1.45×10^9	0.387
10^6	3.64×10^9	6.10	6.71×10^9	1.80
10^7	1.69×10^{10}	28.3	3.12×10^{10}	8.35
10^8	7.85×10^{10}	131	1.45×10^{11}	38.7
10^9	3.64×10^{11}	610	6.71×10^{11}	180
10^{10}	1.69×10^{12}	2 832	3.12×10^{12}	835
10^{11}	7.85×10^{12}	13 143	1.45×10^{13}	3 874

Notes. a is the throat radius of the wormhole, R_E is the Einstein radius, and θ_E is the angular Einstein radius.
[a] $D_S = 8$ kpc and $D_L = 4$ kpc are assumed.
[b] $D_S = 50$ kpc and $D_L = 25$ kpc are assumed.

alone. It is safe to say that the astrometric lensing provides a supplementary method of supporting a photometric detection. First, the impact parameter of the source trajectory $\hat{\beta}_0$ is determined from light curve observations. By using the obtained $\hat{\beta}_0$, one can fit the astrometric observations with wormhole lensing templates. If astrometric data show a better fit with a wormhole case, the detection by light curves will be reinforced. What is more important is that astrometric observations give additional information such as the angular size of the image centroid position shift, so that the degeneracy among (D_L, a, v_T) can be partially broken.

Before closing this section, let us briefly summarize the chain of logic for identifying Ellis lenses. From light curves, first, we distinguish the Ellis lenses from the Schwarzschild ones. The best-fit values of the model parameter combinations are obtained from them. Next, the image centroid observations are used to partially break the parameter degeneracy.

4. SUMMARY

We studied the gravitational microlensing effects of the Ellis wormhole in the weak-field limit. First, we performed a suitable coordinate transformation, such that the lens equation and analytic expressions of the lensed image positions can become much simpler than the previous ones. Second, we proved that two images always appear for the weak-field lens by the Ellis wormhole. By using these analytic results, we investigated astrometric image centroid displacements due to gravitational microlensing by the Ellis wormhole. The anomalous shift of the image centroid by the Ellis wormhole lens is smaller than that by the Schwarzschild lens, provided that the impact parameter and the Einstein ring radius are the same. Therefore, the lensed image centroid by the Ellis wormhole moves slower.

Studies of astrometric image centroid displacements due to another type of wormholes or nontrivial topology of spacetimes are left for future work.

We thank Professor Volker Perlick for invaluable comments on the Ellis wormhole lensing in the strong-field region. This work was supported in part (H.A.) by a Japanese Grant-in-Aid for Scientific Research from the Ministry of Education, No. 21540252.

REFERENCES

Abe, F. 2010, ApJ, 725, 787
Alcock, C., Akerlof, C. W., Allsman, R. A., et al. 1993, Nature, 365, 621
Alcock, C., Allsman, R. A., Alves, D., et al. 1995, ApJ, 454, L125
Alcock, C., Allsman, R. A., Alves, D. R., et al. 2000, ApJ, 542, 281
Alcock, C., Allsman, R. A., Alves, D. R., et al. 2001, ApJ, 550, L169
Asada, H. 2002, ApJ, 573, 825
Asada, H. 2011, Prog. Theor. Phys., 125, 403
Aubourg, E., Bareyre, P., Bréhin, S., et al. 1993, Nature, 365, 623
Beaulieu, J.-P., Bennett, D. P., Fouqué, P., et al. 2006, Nature, 439, 437
Bennett, D. P., Becker, A. C., Quinn, J. L., et al. 2002, ApJ, 579, 639
Bogdanov, M. B., & Cherepashchuk, A. M. 2008, Ap&SS, 317, 181
Bond, I. A., Udalski, A., Jaroszyński, M., et al. 2004, ApJ, 606, L155
Calchi Novati, S., Mancini, L., Scarpetta, G., & Wyrzykowski, Ł. 2009, MNRAS, 400, 1625
Chetouani, L., & Clément, G. 1984, Gen. Rel. Grav., 16, 111
Clément, G. 1984, J. Theor. Phys., 23, 335
Cramer, J. G., Forward, R. L., Morris, M. S., et al. 1995, Phys. Rev. D, 51, 3317
Das, A., & Kar, S. 2005, Class. Quant. Grav., 22, 3045
Dey, T. K., & Sen, S. 2008, Mod. Phys. Lett. A, 23, 953
Einstein, A. 1936, Science, 84, 506
Einstein, A., & Rosen, N. 1935, Phys. Rev., 48, 73
Ellis, H. G. 1973, J. Math. Phys., 14, 104
Gould, A., Udalski, A., Monard, B., et al. 2009, ApJ, 698, L147
Han, C., & Lee, C. 2002, MNRAS, 329, 163
Hosokawa, M., Ohnishi, K., & Fukushima, T. 1997, AJ, 114, 1508
Jeong, Y., Han, C., & Park, S. 1999, ApJ, 511, 569
Liebes, S. 1964, Phys. Rev., 133, 835
Lobo, F. S. N. 2007, in Classical and Quantum Gravity Research, ed. M. N. Christiansen & T. K. Rasmussen (New York: Nova Science Publishers), 1
Miyamoto, M., & Yoshii, Y. 1995, AJ, 110, 1427
Morris, M. S., & Thorne, K. S. 1988, Am. J. Phys., 56, 395
Nandi, K. K., Zhang, Y.-Z., & Zakharov, A. V. 2006, Phys. Rev. D, 74, 024020
Nemiroff, R. J., & Wickramasinghe, W. A. D. T. 1994, ApJ, 424, L21
Paczyński, B. 1986, ApJ, 304, 1
Perlick, V. 2004, Phys. Rev. D, 69, 064017
Poindexter, S., Afonso, C., Bennett, D. P., et al. 2005, ApJ, 633, 914
Rahaman, F., Kalam, M., & Chakraborty, S. 2007, Chin. J. Phys., 45, 518
Refsdal, S. 1964, MNRAS, 128, 295
Safizadeh, N., Dalal, N., & Griest, K. 1999, ApJ, 522, 512
Safonova, M., Diego, F. T., & Romero, G. E. 2002, Phys. Rev. D, 65, 023001
Schneider, P., Ehlers, J., & Falco, E. E. 1992, Gravitational Lenses (New York: Springer)
Shatskiĭ, A. A. 2004, Astron. Rep., 48, 525
Shinkai, H., & Hayward, S. A. 2002, Phys. Rev. D, 66, 044005
Tisserand, P., Le Guillou, L., Afonso, C., et al. 2007, A&A, 469, 387
Torres, D. F., Romero, G. E., & Anchordoqui, L. A. 1998, Phys. Rev. D, 58, 123001
Udalski, A., Szymanski, M., Kaluzny, J., et al. 1993, Acta Astron., 43, 289
van der Waerden, B. L. 1966, Algebra I (Berlin: Springer)
Visser, M. 1995, Lorentzuan Wormholes: From Einstein to Hawking (New York: AIP)
Walker, M. A. 1995, ApJ, 453, 37
Wyrzykowski, Ł., Kozłowski, S., Skowron, J., et al. 2009, MNRAS, 397, 1228